Drastic Difference in Lifetimes of the Charge-Separated State of the Formanilide−Anthraquinone Dyad versus the Ferrocene−Formanilide−Anthraquinone Triad and Their Photoelectrochemical Properties of the Composite Films with Fullerene Clusters

Ken Okamoto,[†] Taku Hasobe,[†,‡] Nikolai V. Tkachenko,[§] Helge Lemmetyinen,*[,§] Prashant V. Kamat,*[,‡] and Shunichi Fukuzumi*[,†,||]

Department of Material and Life Science, Graduate School of Engineering, Osaka University, SORST, Japan Science and Technology Agency, Suita, Osaka 565-0871, Japan, The Institute of Materials Chemistry, Tampere University of Technology, P.O. Box 541, FIN-33101 Tampere, Finland, and Notre Dame Radiation Laboratory, University of Notre Dame, Notre Dame, Indiana 46556-0579

Received: October 30, 2004; In Final Form: February 11, 2005

A long-lived charge-separated (CS) state, which can be observed even at 900 μs after laser excitation, has been attained in the formanilide−anthraquinone dyad (**FA-AQ**) in dimethyl sulfoxide, whereas the CS lifetime is shortened significantly to 20 ps in the ferrocene−formanilide−anthraquinone triad (**Fc-FA-AQ**). Such a drastic decrease in the CS lifetime by the addition of a ferrocene moiety to the **FA-AQ** dyad is ascribed to a decrease in the driving force of back electron transfer and an increase in the reorganization energy of electron transfer despite the longer charge-separation distance. The **FA-AQ** dyad and the **Fc-FA-AQ** triad have been employed as components of photovoltaic cells, where composite molecular nanoclusters of the **FA-AQ** dyad or the **Fc-FA-AQ** triad with fullerene (C_{60}) are assembled onto a SnO_2 electrode using an electrophoretic method. The composite films of the **Fc-FA-AQ** triad exhibit 10 times smaller values of an incident photon-to-photocurrent efficiency (IPCE) as compared with those of the **FA-AQ** dyad in accordance with a drastic decrease of the CS lifetime by addition of a ferrocene moiety to the **FA-AQ** dyad.

Introduction

The most common strategy to achieve long-lived charge-separated (CS) states makes use of multistep short-range photoinduced electron-transfer reactions along well-designed redox gradients.[1−11] The natural photosynthetic reaction center executes such multistep photoinduced electron-transfer processes to attain the final CS state with a long lifetime ($\tau = \sim$1 s) as well as with unit efficiency.[1] The resulting CS energy is effectively converted into chemical energy.[1] However, it should be noted that a significant amount of energy is lost during the multistep electron-transfer processes, because each step loses a fraction of the initial excitation energy. Theoretically it is possible to attain a long-lived CS state by a one-step photoinduced electron transfer in a donor (D)−acceptor (A) dyad provided that the driving force of charge recombination ($-\Delta G_{CR}$) is much larger than the reorganization energy (λ) of electron transfer, because the charge recombination (CR) rate is expected to decrease with an increase of the driving force in the Marcus inverted region: $-\Delta G_{CR} > \lambda$.[12] In most cases, however, it has been difficult to realize such a situation because of the low-lying excited state of a donor or acceptor component, which can intercept the back electron-transfer process to the ground state. In this context, we have designed and synthesized simple D-A dyads which have higher local excited states than the CS states to attain extremely long-lived CS states.[13,14] Simple D-A dyads, which have long-lived CS states, have great advantages with regard to synthetic feasibility and practical applications as compared with the more sophisticated molecular triad, tetrad, pentad, and so forth. When a dyad is extended to a triad, the longer charge-separation distance in the triad as compared with the dyad usually results in a decrease in the electron coupling term, leading to an increase in the CS lifetime.[10,11] If the CR process of a dyad is deeply in the Marcus inverted region, however, the extension of a dyad to a triad results in less driving force of the CR process, which would lead to a decrease in the CS lifetime despite the longer charge-separation distance. Such a decrease in the CS lifetime from a dyad to the corresponding triad has yet to be reported.

CHART 1

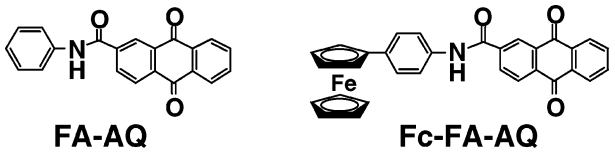

We report herein a drastic decrease in the CS lifetime from a simple D-A dyad to a triad (D′-D-A). The simple dyad employed in this study is the formanilide−anthraquinone dyad (**FA-AQ**), to which ferrocene is connected to afford the triad (**Fc-FA-AQ**) as shown in Chart 1. An extremely long-lived CS state, which can be observed even at 900 μs after laser excitation, has been attained in **FA-AQ**, whereas the triad **Fc-FA-AQ** has an extremely short CS lifetime (20 ps). Such a drastic difference in the CS lifetimes is shown to be well-reflected in the

* Authors to whom correspondence should be addressed.
[†] Osaka University, SORST, Japan Science and Technology Agency.
[‡] University of Notre Dame.
[§] Tampere University of Technology.
[||] E-mail: fukuzumi@ap.chem.eng.osaka-u.ac.jp.

10.1021/jp045042e CCC: $30.25
Published on Web 05/05/2005

photoelectochemical properties of the composite films of **FA-AQ** and **Fc-FA-AQ** with fullerene clusters.

Experimental Section

Materials. All solvents and chemicals were of reagent grade quality, obtained commercially and used without further purification unless otherwise noted. Thin-layer chromatography (TLC) and flash column chromatography were performed with Art. 5554 DC-Alufolien Kieselgel 60 F_{254} (Merck), and Fujisilica BW300, respectively. Nanostructured SnO_2 films were cast on an optically transparent electrode (OTE) by applying a 2% colloidal solution obtained from Alfa Chemicals. The air-dried films were annealed at 673 K. The details of the preparation of SnO_2 films on conducting glass substrate were reported elsewhere.[15] The SnO_2 film electrode is referred as OTE/SnO_2. Dimeric 1-benzyl-1,4-dihydronicotinamide [$(BNA)_2$] was prepared according to the literature.[16] The synthesis and characterization of the **FA-AQ** dyad and the **Fc-FA-AQ** triad were reported previously.[17]

Spectral Measurements. The one-electron reduced species, **FA-AQ**$^{\bullet-}$ and **Fc-FA-AQ**$^{\bullet-}$, were produced by the chemical reduction of **FA-AQ** and **Fc-FA-AQ** with the naphthalene radical anion generated by naphthalene (0.5 g) in THF with sodium (0.075 g), respectively. The concentration of the naphthalene radical anion was determined by the appearance of the absorption band at the characteristic peak of the *p*-benzosemiquinone radical anion [$\epsilon(422\ \text{nm}) = 6.0 \times 10^3\ \text{M}^{-1}\ \text{cm}^{-1}$ in MeCN] produced by the titration of the naphthalene radical anion to *p*-benzoquinone. The spectral measurements were performed on a Hewlett-Packard 8453 diode array spectrophotometer with a quartz cuvette (path length = 10 mm) at 298 K.

Time-Resolved Absorption Measurements. Femtosecond-to-picosecond time-resolved absorption spectra were collected using a pump−probe technique as described elsewhere.[18] The femtosecond pulses of the Ti:sapphire generator were amplified by using a multipass amplifier (CDP-Avesta, Moscow, Russia) pumped by a second harmonic of the Nd:YAG Q-switched laser (model LF114, Solar TII, Minsk, Belorussia). The amplified pulses were used to generate a second harmonic (420 nm) for sample excitation (pump beam) and white continuum for time-resolved spectrum detection (probe beam). The samples were placed into 1-mm rotating cuvettes, and averaging of 100 pulsed at 10 Hz repetition rate was used to improve the signal-to-noise ratio. Typical response time of the instrument was 150 fs (fwhm). A global multiexponential fitting procedure was applied to process the data. The procedure takes into account the instrument time response function and the group velocity dispersion of the white continuum and allowed calculation of the decay time constants and dispersion-compensated transient absorption spectra. Nanosecond transient absorption measurements were carried out using a Nd:YAG laser (Solar, TII) at 355 nm as an excitation source. The solution was deoxygenated by argon purging for 15 min prior to the measurements.

The quantum yields were measured using the comparative method.[19] In particular, the strong fullerene triplet−triplet absorption (788 nm = 18800 $\text{M}^{-1}\ \text{cm}^{-1}$ in benzene; $\phi_T = 0.98$)[19] served as a probe to obtain the quantum yields for the CS state.

Electrochemical Measurements. Electrochemical measurements were performed on a BAS 100W electrochemical analyzer in deaerated DMSO containing 0.1 M Bu_4NPF_6 ($TBAPF_6$) as supporting electrolyte at 298 K. A conventional three-electrode cell was used with a platinum working electrode (surface area of 0.3 mm^2) and a platinum wire as the counter electrode. The Pt working electrode (BAS) was routinely polished with a BAS polishing alumina suspension and rinsed with acetone before use. The measured potentials were recorded with respect to the $Ag/AgNO_3$ (0.01 M) reference electrode. The second-harmonic alternating current voltammetry (SHACV) measurements were carried out with a BAS 100B electrochemical analyzer in deaerated DMSO containing 0.1 M Bu_4NPF_6 ($TBAPF_6$) as supporting electrolyte.[20] All potentials (vs Ag/Ag^+) were converted to values vs SCE by adding 0.29 V.[21] All electrochemical measurements were carried out under an atmospheric pressure of Ar.

Electrophoretic Deposition of Cluster Films. An aliquot (∼2 mL) of a mixed acetonitrile/toluene (3:1, v/v) solution of **FA-AQ** (or **Fc-FA-AQ**) and C_{60} clusters was transferred to a 1-cm cuvette in which two electrodes (i.e., OTE/SnO_2 and OTE; optically transparent electrodes) were kept at a distance of ∼6 mm using a Teflon spacer. A dc voltage (500 V) for 2 minutes was applied between these two electrodes using a Fluke 415 power supply. The deposition of the film can be visibly seen as the solution becomes colorless with simultaneous dark brown coloration of the SnO_2/OTE electrode. The SnO_2/OTE electrodes coated with **FA-AQ**/C_{60} clusters or **Fc-FA-AQ**/C_{60} clusters are referred to as OTE/SnO_2/(**FA-AQ**+C_{60})$_n$ and OTE/SnO_2/ (**Fc-FA-AQ**+C_{60})$_n$, respectively.

The UV−vis spectra were recorded on a Shimadzu 3101 or a Cary 50 spectrophotometer. Transmission electron micrographs (TEM) of C_{60} clusters were recorded by applying a drop of the sample to a carbon-coated copper grid. Images were recorded using a Hitachi H600 transmission electron microscope.

Photoelectrochemical Measurements. Photoelectrochemical measurements were carried out in a standard three-compartment cell consisting of a working electrode, a Pt wire gauze counter electrode, and a saturated calomel reference electrode (SCE). This configuration allowed us to carry out photocurrent measurements under electrochemical bias. A Princeton Applied Research (PAR) model 173 potentiostat and model 175 universal programmer were used for recording $I-V$ characteristics. All other photoelectrochemical measurements were carried out using a Pt gauge counter electrode in the same cell assembly using a Keithley model 617 programmable electrometer. The electrolyte was 0.5 M NaI and 0.01 M I_2 in acetonitrile. A collimated light beam from a 150 W xenon lamp with a 370 nm cutoff filter was used for excitation of (**FA-AQ**+C_{60})$_n$ and (**Fc-FA-AQ**+C_{60})$_n$ films cast on SnO_2 electrodes. A Bausch and Lomb high-intensity grating monochromator was introduced into the path of the excitation beam for the selected wavelength.

ESR Measurements. A quartz ESR tube (internal diameter: 4.5 mm) containing a deaerated acetonitrile/toluene (3:1, v/v) solution of (**FA-AQ**+C_{60})$_n$ or (**Fc-FA-AQ**+C_{60})$_n$ or a DMSO solution of **FA-AQ** was irradiated in the cavity of the ESR spectrometer with the focused light of a 1000-W high-pressure Hg lamp (Ushio-USH1005D) through an aqueous filter at low temperature. The ESR spectra in frozen acetonitrile/toluene were measured under nonsaturating microwave power conditions using a JEOL X-band spectrometer (JES-RE1XE) with an attached variable temperature apparatus. The *g* values were calibrated with an Mn^{2+} marker.

Theoretical Calculations. Density-functional theory (DFT) calculations were performed on a COMPAQ DS20E computer. Geometry optimizations were carried out using the Becke3LYP functional and 6-31G(d) basis set[22] with the restricted Hatree-Fock (RHF) formalism and as implemented in the Gaussian 98 program.[23] Graphical output of the computational results were

TABLE 1: Redox Potentials, Driving Forces of CS ($-\Delta G_{CS}$) and CR ($-\Delta G_{CR}$), Lifetimes of CS (τ_{CS}) and CR (τ_{CR})

dyad (D-A)	E^0_{OX}, V[a] $D^{\bullet+}/D$	E^0_{red}, V[a] $A/A^{\bullet-}$	$-\Delta G_{CS}$, eV[b]	$-\Delta G_{CR}$, eV	τ_{CR}	τ_{CS}[b]
FA-AQ	1.37	−0.87	0.21	2.24	>900 μs	1.7 ps
Fc-FA-AQ	0.30	−0.86	1.29	1.16	20 ps	0.7 ps

[a] vs SCE. [b] CS from ^{3}AQ* to FA or Fc.

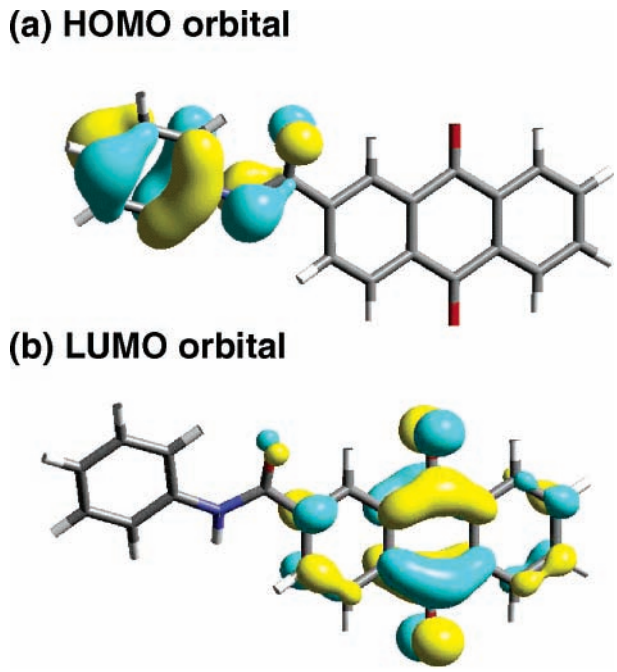

Figure 1. (a) HOMO and (b) LUMO orbitals of the **FA-AQ** dyad calculated by a DFT method with Gaussian 98 (B3LYP 6-31G(d) basis set).

generated with the Cerius[2] software program developed by Molecular Simulations Inc.

Results and Discussion

Photodynamics of the FA-AQ Dyad. The one-electron oxidation (E^0_{ox}) and reduction (E^0_{red}) potentials of the **FA-AQ** dyad were determined by cyclic voltammetry and second harmonic AC votammetry (SHACV) as 1.37 V and −0.87 V vs SCE, respectively (see Experimental Section). The driving forces of CS ($-\Delta G_{CS}$) and CR ($-\Delta G_{CR}$) are summarized in Table 1, where $-\Delta G_{CS}$ for electron transfer from the formanilide (FA) moiety to the triplet excited state of anthraquinone moiety (^{3}AQ*) is determined by subtracting the $-\Delta G_{CR}$ value from the triplet excited energy (^{3}AQ* = 2.45 eV).[24] The $-\Delta G_{CR}$ value of **FA-AQ** (2.24 eV) is smaller than the singlet and triplet excited energy of each moiety of the dyad.[24]

The HOMO and LUMO orbitals of the **FA-AQ** dyad are calculated by a DFT method with Gaussian 98 (B3LYP 6-31G-(d) basis set) as shown in Figure 1, where the HOMO orbital is localized on the FA moiety, whereas the LUMO orbital is localized on the AQ moiety. Thus, photoinduced electron transfer from the FA moiety to the AQ moiety in the **FA-AQ** dyad is expected to produce the CS state (**FA$^{\bullet+}$-AQ$^{\bullet-}$**).

The occurrence of photoinduced electron transfer in the **FA-AQ** dyad and formation of the CS state (**FA$^{\bullet+}$-AQ$^{\bullet-}$**) was confirmed by the femtosecond pump−probe measurements (see Experimental Section). Transient component spectra of **FA-AQ** in DMSO ($-\Delta G_{CR}$ = 2.24 eV) obtained by femtosecond pump−probe measurements (excitation at 420 nm) are shown with the lifetimes of 0.4, 1.7, and ≫ 50 ps in Figure 2. The singlet excited

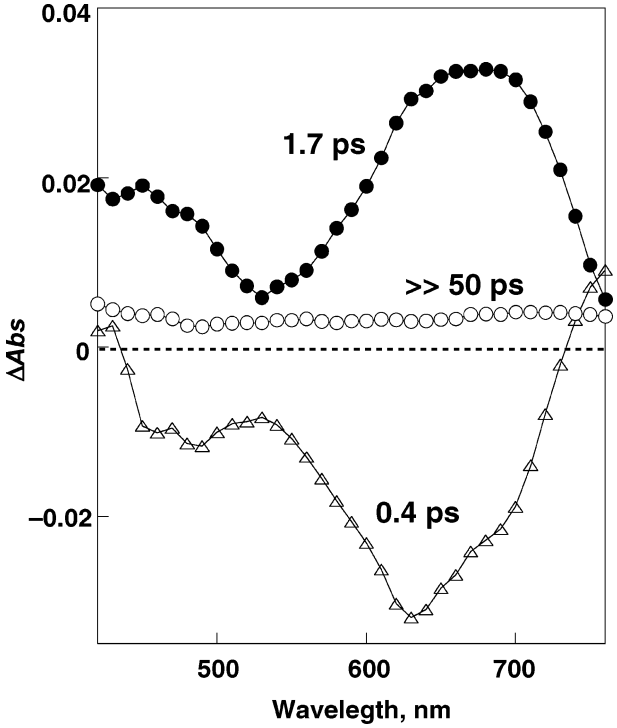

Figure 2. Time-resolved transient component spectra of **FA-AQ** with lifetimes 0.45 ps (△), 1.7 ps (●), and ≫50 ps (○) obtained by global three-exponential fit, photoexcitation at 420 nm in DMSO at 298 K.

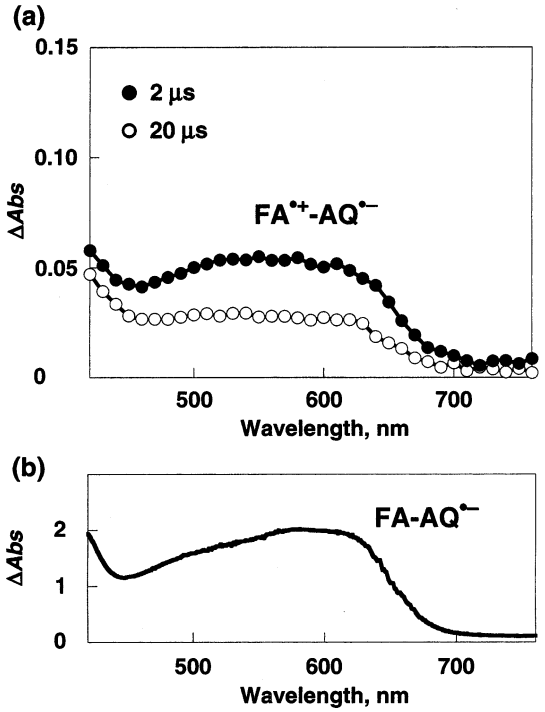

Figure 3. (a) Time-resolved absorption spectra of **FA-AQ** (2.0×10^{-5} M) in deaerated DMSO at 298 K after photoexcitation at 355 nm [delay time: 2 μs (●), 20 μs (○)]. (b) Absorption spectrum of **FA-AQ$^{\bullet-}$** (1.0×10^{-4} M) produced by the chemical reduction of **FA-AQ** with the naphthalene radical anion in deaerated DMSO at 298 K.

state (^{1}AQ*) after excitation has an absorption band around 720 nm (not shown) with the lifetime of 0.4 ps. The singlet state absorption at 720 nm is transformed to a new absorption at 690 nm as indicated by the mirror image of the component spectra in Figure 2 with the lifetime of 0.4 ps.[25] The observed rate constants are virtually the same as the reported rate constants of ISC (intersystem crossing) processes of quinone derivatives.[26]

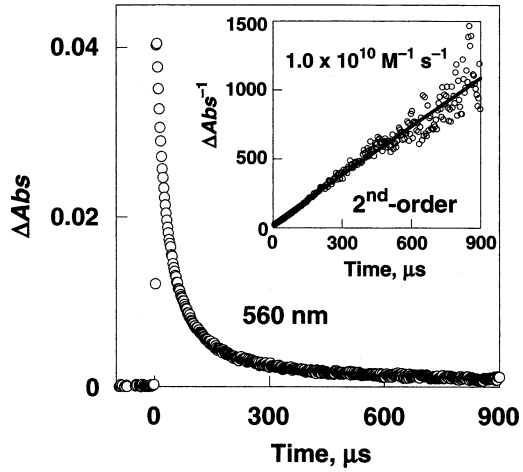

Figure 4. Decay time profile of **FA-AQ** (2.0×10^{-5} M) in deaerated DMSO at 298 K after photoexcitation at 355 nm monitored at 560 nm. Inset: Second-order plot.

In fact, the transient component spectrum with the lifetime of 1.7 ps (Figure 2) is similar to the reported triplet−triplet (T−T) absorption spectrum of AQ (monosubstituted AQ in 2-position).[27] Thus, the transient component spectrum at 1.7 ps corresponds to the AQ T−T relaxation, accompanied by electron transfer from the FA moiety to the ^{3}AQ* (2.45 eV) moiety. The transient component spectrum at ≫ 50 ps indicates the CS state of **FA**$^{\bullet+}$-**AQ**$^{\bullet-}$, where the transient absorption spectrum in the longer wavelength (500−700 nm) may be ascribed to the CS state, although the small absorption compared to the strong ^{3}AQ* absorption has precluded the definitive assignment.

The transient absorption spectrum of the long-lived component detected in the femtosecond pump−probe measurements is now clearly observed by nanosecond laser flash photolysis as shown in Figure 3a. Transient absorption spectra of a DMSO solution of **FA-AQ** ($-\Delta G_{CR} = 2.24$ eV) observed at 2 μs and 20 μs after the laser pulse excitation (355 nm) agrees with the absorption band of **FA-AQ**$^{\bullet-}$, which was produced independently by the one-electron reduction of **FA-AQ** with the naphthalene radical anion (Figure 3b). The absorption spectra of semiquinone radical anions are known to be significantly red-shifted as compared with those of the corresponding neutral semiquinone radicals.[28] For example, the anthraquinone radical anion (AQ$^{\bullet-}$) has an absorption maximum at 543 nm,[29] whereas the absorption maximum of the neutral semiquinone radical (the protonated form: AQH$^{\bullet}$) appears at 500 nm.[30] In the case of **FA-AQ**$^{\bullet-}$ the absorption maximum (ca. 600 nm) is further red-shifted as compared with that of AQ$^{\bullet-}$.[31] Thus, the long-lived transient absorption spectra in Figure 3a can be safely assigned to the CS state: **FA**$^{\bullet+}$-**AQ**$^{\bullet-}$.[32] The decay process of the CS state obeys second-order kinetics at 560 nm due to AQ$^{\bullet-}$ rather than the usual first-order kinetics as shown in Figure 4. From the second-order plot (inset of Figure 4), the second-order rate constant was determined as 1.0×10^{10} M^{-1} s^{-1}, which is close to the diffusion-limited value.[33] Such a second-order decay indicates that the process of intramolecular charge-recombination (CR) is much slower than that of intermolecular CR between two CS molecules as observed for donor−acceptor dyads which have extremely long lifetimes.[11,14] The slow CR rate comes from the large driving force of the back electron transfer in **FA**$^{\bullet+}$-**AQ**$^{\bullet-}$ ($-\Delta G_{CR} = 2.24$ eV), which is deep in the Marcus inverted region, where the intramolecular CR rate decreases with an increase of the driving force.[12−14] In the case of intermolecular CR, the larger solvent reorganization as compared with that of the intramolecular CR in the CS state with a short linkage results

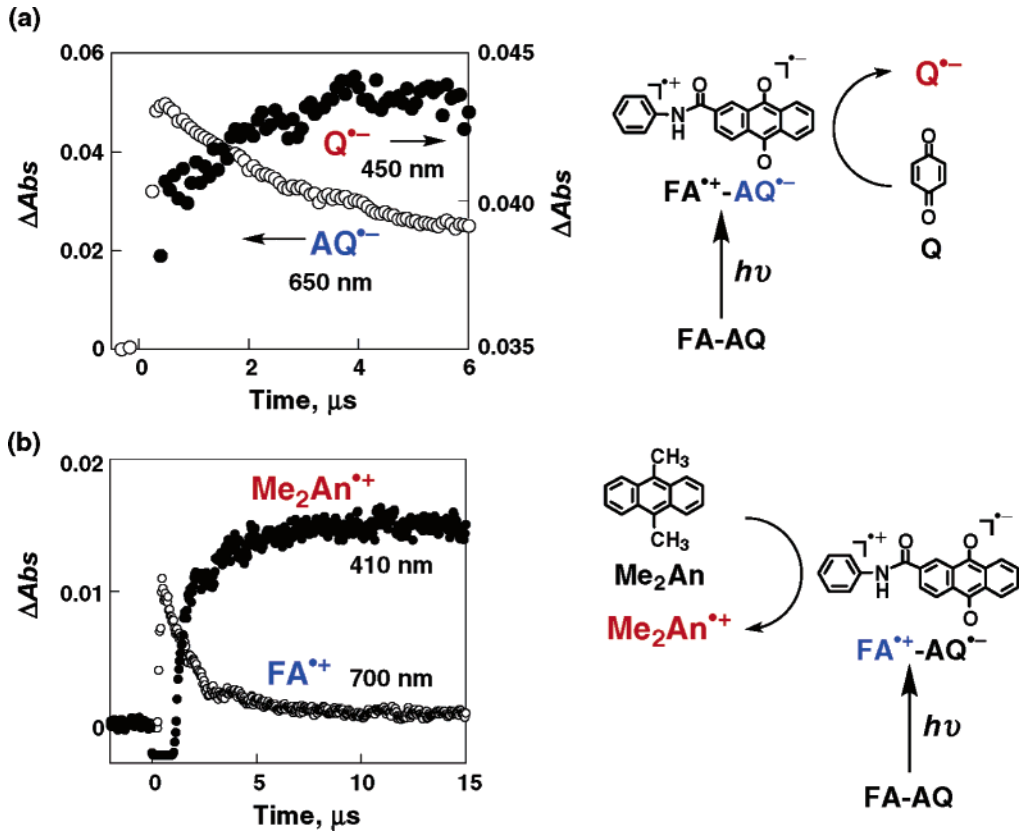

Figure 5. (a) Time profiles of the absorption decay at 650 nm (○) and the rise at 450 nm (●) for electron transfer from AQ$^{\bullet-}$ of the CS state of **FA-AQ** (2.0×10^{-5} M) to *p*-benzoquinone (Q, 6.0×10^{-4} M), and (b) time profiles of the absorption decay at 700 nm (○) and the rise at 410 nm (●) for electron transfer from 9,10-dimethylanthracene (Me_2An, 2.0×10^{-4} M) to FA$^{\bullet+}$ of the CS state of **FA-AQ** (2.0×10^{-5} M) after photoexcitation at 355 nm in deaerated DMSO at 298 K.

in the faster CR rate, since the CR rate decreases with an increase of the reorganization energy in the Marcus inverted region.[12−14]

The existence of $AQ^{\bullet-}$ in the CS state of **FA-AQ** has been further examined by an intermolecular electron transfer from $\mathbf{FA}^{\bullet+}$-$\mathbf{AQ}^{\bullet-}$ to *p*-benzoquinone (Q). This is shown in Figure 5a, where the rise time profile of absorbance at 450 nm due to formation of $Q^{\bullet-}$, observed after photoexcitation of **FA-AQ** in the presence of Q, coincides with the decay time profile of absorbance at 650 nm due to $AQ^{\bullet-}$. The existence of $FA^{\bullet+}$ in the CS state has also been confirmed by the addition of 9,10-dimethylanthracene (Me_2An) to the **FA-AQ** system as shown in Figure 5b, where the rise time profile of absorbance at 410 nm due to $Me_2An^{\bullet+}$ coincides with the decay time profile at 700 nm due to $FA^{\bullet+}$.[34]

The quantum yield of the CS state in **FA-AQ** was determined as 74% using the comparative method (see Experimental Section).[19]

Photodynamics of the Fc-FA-AQ Triad. The ferrocene moiety was attached to **FA-AQ** to afford the triad (**Fc-FA-AQ**) in Chart 1. The one-electron oxidation potential (E^0_{ox}) of **Fc-FA-AQ** was determined as 0.30 V vs SCE for the Fc^+/Fc redox couple by the CV measurement, which is much lower than the E^0_{ox} (1.37 V) of **FA-AQ** for the $FA^{\bullet+}$/FA couple as shown in Table 1, whereas the one-electron reduction potential (E^0_{red} = −0.86 V) for $AQ/AQ^{\bullet-}$ in **Fc-FA-AQ** is virtually the same as the E^0_{red} (−0.87 V) in **FA-AQ**. Thus, the CS energy in $\mathbf{Fc}^+$-$\mathbf{FA\text{-}AQ}^{\bullet-}$ (1.16 eV) is much smaller than that in **FA-AQ** (2.24 eV).

Transient component spectra of a DMSO solution of **Fc-FA-AQ** obtained by the femtosecond pump−probe measurements are shown in Figure 6. The transient component spectrum due to ^{1}AQ* with the lifetime of 0.2 ps is transformed to that due to ^{3}AQ*, as indicated by the mirror image of the component spectra in Figure 6a as is the case of **FA-AQ** in Figure 2a.[35] The lifetime of the ^{3}AQ* moiety in **Fc-FA-AQ** (0.7 ps) in Figure 6a is significantly shorter than the corresponding ^{3}AQ* lifetime in **FA-AQ** (1.7 ps) in Figure 2a. This indicates that ^{3}AQ* decays mainly via direct electron transfer from the Fc moiety to ^{3}AQ* in addition to that from FA to ^{3}AQ*.[36] The CS time constants (τ_{CS}) of **Fc-FA-AQ** and **FA-AQ** are listed in Table 1. The faster CS process of **Fc-FA-AQ** may result from the larger driving force ($-\Delta G_{CS}$ = 1.29 eV) as compared with that of **FA-AQ** ($-\Delta G_{CS}$ = 0.21 eV).

The transient spectrum with the lifetime of 20 ps corresponds to the CS state ($\mathbf{Fc}^+$-$\mathbf{FA\text{-}AQ}^{\bullet-}$) by the comparison with the absorption band due to $\mathbf{Fc\text{-}FA\text{-}AQ}^{\bullet-}$, which was generated by the chemical reduction of **Fc-FA-AQ**, where Fc^+ has much lower extinction coefficient than $AQ^{\bullet-}$.[37] The short lifetime of $\mathbf{Fc}^+$-$\mathbf{FA\text{-}AQ}^{\bullet-}$ (τ_{CR} = 20 ps in Table 1) shows sharp contrast to the long lifetime of $\mathbf{FA}^{\bullet+}$-$\mathbf{AQ}^{\bullet-}$, in which the intermolecular CR process predominates over the intramolecular slow CR process (vide supra). The fast CR rate in $\mathbf{Fc}^+$-$\mathbf{FA\text{-}AQ}^{\bullet-}$ comes from the small CR driving force ($-\Delta G_{CR}$ = 1.16 eV) being close to the Marcus top region, as compared with the large CR driving force in $\mathbf{FA}^{\bullet+}$-$\mathbf{AQ}^{\bullet-}$ ($-\Delta G_{CR}$ = 2.24 eV), which is deep in the Marcus inverted region. In fact, the reorganization energy of self-exchange electron transfer of ferrocene (1.0 eV)[38] is close to the CR driving force in $\mathbf{Fc}^+$-$\mathbf{FA\text{-}AQ}^{\bullet-}$ ($-\Delta G_{CR}$ = 1.16 eV), whereas the reorganization energy of self-exchange electron transfer of aromatic amines (0.5 eV)[39] is much smaller than the CR driving force in $\mathbf{FA}^{\bullet+}$-$\mathbf{AQ}^{\bullet-}$ ($-\Delta G_{CR}$ = 2.24 eV).

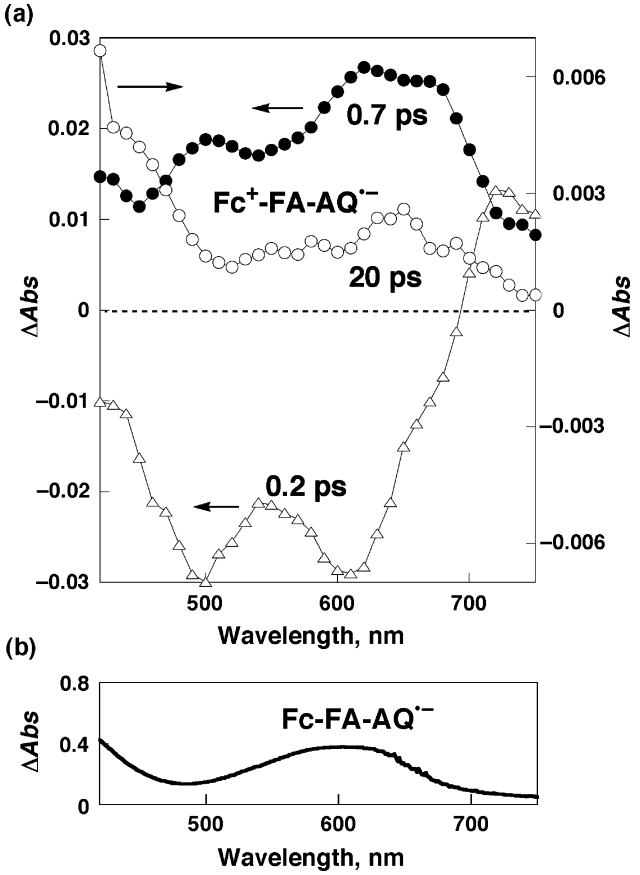

Figure 6. (a) Time-resolved component spectra of **Fc-FA-AQ** (1.0×10^{-4} M) in DMSO at 298 K after photoexcitation at 420 nm [lifetimes: 0.2 ps (△), 0.7 ps (●), 20 ps (○)]. (b) Absorption spectrum of $\mathbf{Fc\text{-}FA\text{-}AQ}^{\bullet-}$ (4.0×10^{-5} M) produced by the chemical reduction of **Fc-FA-AQ** with the naphthalene radical anion in deaerated DMSO at 298 K.

Clusterization of the FA-AQ Dyad and the Fc-FA-AQ Triad with C_{60} in Mixed Solvent. The **FA-AQ** dyad with a fast CS process and a long-lived CS state was employed as a component of photovoltaic cells, where composite molecular nanoclusters of the **FA-AQ** dyad and fullerene (C_{60}) were assembled onto a SnO_2 electrode using an electrophoretic method. For comparison, the **Fc-FA-AQ** triad with a fast CS process and a short-lived CS state was also employed as a component of photovoltaic cells, where composite molecular nanoclusters of the **Fc-FA-AQ** triad and fullerene (C_{60}) were assembled onto a SnO_2 electrode using an electrophoretic method. **FA-AQ**, **Fc-FA-AQ**, and C_{60} are soluble in toluene, but they are insoluble in acetonitrile. When a concentrated solution of **FA-AQ** (or **Fc-FA-AQ**) and C_{60} in toluene is mixed with acetonitrile by a fast injection method, the molecules aggregate to form stable clusters.[40] The final solvent ratio of mixed solvent was 3:1 (v/v) acetonitrile/toluene. Mixed cluster aggregates were prepared by mixing equimolar solution of **FA-AQ** (or **Fc-FA-AQ**) and C_{60} in toluene (0.5 mL) and then injecting into a pool of acetonitrile (1.5 mL). These optically transparent composite clusters are stable at room temperature and they can be reverted back to their monomeric forms by diluting the solution with toluene.[40−42]

The absorption spectra of **FA-AQ** and C_{60} in their clusters form in acetonitrile/toluene (3:1, v/v) are compared with the absorption spectrum of $[(\mathbf{FA\text{-}AQ}+C_{60})_n]$ clusters together with $[(\mathbf{Fc\text{-}FA\text{-}AQ}+C_{60})_n]$ clusters in acetonitrile/toluene (3:1, v/v) in Figure 7a. The composite clusters $[(\mathbf{FA\text{-}AQ}+C_{60})_n]$ in the mixed solvent exhibit more intense absorption in the visible

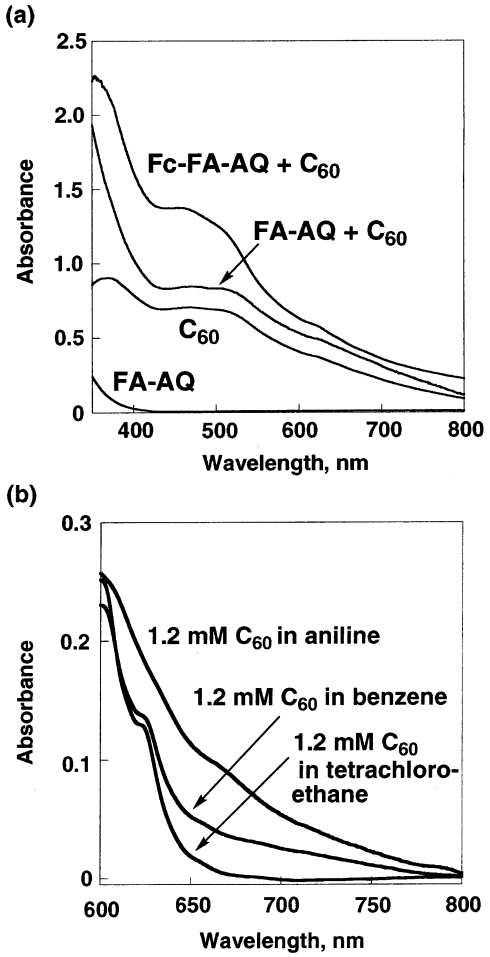

Figure 7. (a) Absorption spectra of (**Fc-FA-AQ**+C_{60}), (**FA-AQ**+C_{60}), C_{60}, and **FA-AQ** in its monomer and cluster forms in acetonitrile/toluene (3:1, v/v); [**FA-AQ**] = [**Fc-FA-AQ**] = [C_{60}] = 0.31 mM. (b) Absorption spectra of 1.2 mM C_{60} in aniline, benzene, and tetrachloroethane.

and near-infrared regions than individual clusters of C_{60}. A charge transfer (CT) type interaction between the donor (FA) moiety and the acceptor (C_{60}) may be responsible for the long-wavelength absorption of the composite clusters in Figure 7a.[43,44] To confirm the CT interaction between the donor and C_{60}, the absorption spectra of 1.2 mM C_{60} in tetrachloroethane, benzene, and aniline were observed as shown in Figure 7b. The absorption in the longer wavelength (600−800 nm) increases following the sequence: in tetrachloroethane, benzene, and aniline, in accordance with an increase in the electron donor ability of the solvent. Figure 8 shows transmission electron micrograph (TEM) images of the composite clusters, (**FA-AQ**+C_{60})$_n$, (**FA-AQ**+C_{60})$_n$, and (C_{60})$_n$.

As the solvents evaporate on the copper grid the clusters form microcrystallites of well-defined shapes. The interaction between **FA-AQ** and C_{60} (Figure 8a) or **Fc-FA-AQ** and C_{60} (Figure 8b) in the aggregated clusters plays an important role in dictating the growth of the microcrystallites, where those composite clusters have larger sizes with a networked structure than the C_{60} clusters (Figure 8c).[41,42] The composite clusters [(**Fc-FA-AQ**+C_{60})$_n$] in Figure 7a also show intense absorption in the visible and near-infrared regions in the same manner as that of [(**FA-AQ**+C_{60})$_n$], which indicates CT interaction in [(**Fc-FA-AQ**+C_{60})$_n$] clusters in accordance with the TEM images.

Electrophoretic Deposition of the FA-AQ Dyad and the Fc-FA-AQ Triad with C_{60} Nanoclusters. The C_{60} clusters

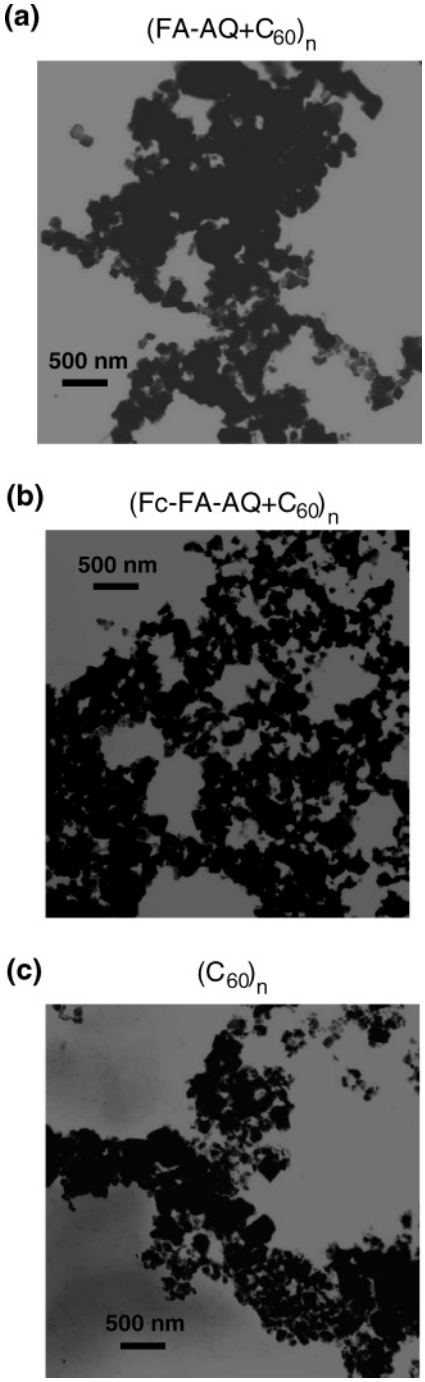

Figure 8. (a) Transmission electron micrographs of clusters prepared with [**FA-AQ**] = [C_{60}] = 0.31 mM, (b) prepared with [**Fc-FA-AQ**] = [C_{60}] = 0.31 mM, and (c) prepared with [C_{60}] = 0.31 mM in acetonitrile/toluene (3:1, v/v).

prepared in acetonitrile/toluene mixed solvent can be assembled electrophoretically as thin films on a conducting glass electrode surface.[40,41] Such an electrodeposition method was adopted to prepare film of (**FA-AQ**+C_{60})$_n$ and (**Fc-FA-AQ**+C_{60})$_n$ on nanostructured SnO_2 films, which were cast on an optically conducting glass electrode (referred to as OTE/SnO_2). Upon application of the dc electric field of 500 V between OTE/SnO_2 and OTE electrodes which were immersed in parallel in a mixed acetonitrile/toluene (3:1, v/v) solution containing (**FA-AQ**+C_{60})$_n$ and (**Fc-FA-AQ**+C_{60})$_n$ clusters, mixed clusters were deposited on SnO_2 nanocrystallites. As the deposition continues we can visually observe discoloration of the solution and coloration of the electrode that is connected to positive terminal of the dc

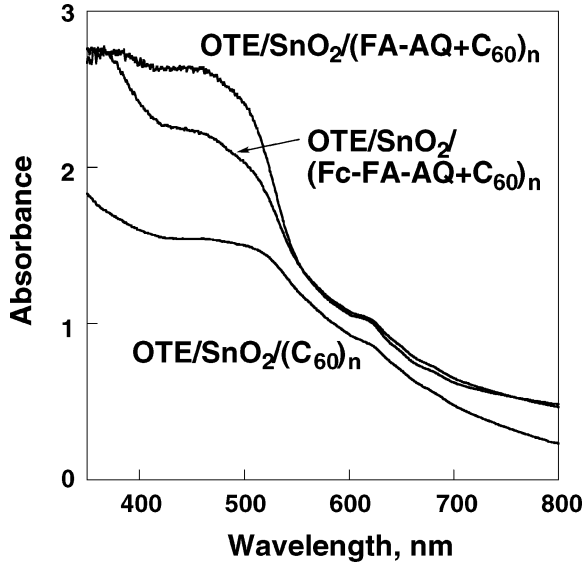

Figure 9. Absorption spectra of electrophoretically deposited OTE/SnO_2/(**FA-AQ**+C_{60})$_n$, OTE/SnO_2/(**Fc-FA-AQ**+C_{60})$_n$, OTE/SnO_2/(C_{60})$_n$ films at an applied voltage of 500 V dc for 1 min ([**FA-AQ**] = [**Fc-FA-AQ**] = [C_{60}] = 0.31 mM).

SCHEME 1: Construction of Photocurrent Generation Systems Using Dyad or Triad/C_{60} Mixed Nanoclusters

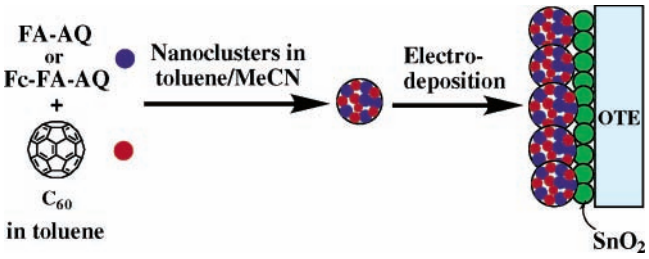

power supply. Figure 9 shows the absorption spectra of OTE/SnO_2/(**FA-AQ**+C_{60})$_n$, OTE/SnO_2/(**Fc-FA-AQ**+C_{60})$_n$, and OTE/SnO_2/(C_{60})$_n$ electrodes prepared using different precursor concentrations of **FA-AQ** or **Fc-FA-AQ** and C_{60} in an acetonitrile/toluene (3:1, v/v) mixture. An increase in absorbance of OTE/SnO_2/(**FA-AQ**+C_{60})$_n$ and OTE/ SnO_2/(**Fc-FA-AQ**+C_{60})$_n$ in the visible and near-infrared regions is evident from Figure 9 as compared with that of OTE/SnO_2/(C_{60})$_n$ without the dyad or the triad. The formation of composite nanoclusters in mixed solvents and their growth as microcrystallites are illustrated in Scheme 1.

Photoelectrochemical Properties of Photovoltaic Cells. To evaluate the photoelectrochemical performance of the (**FA-AQ**+C_{60})$_n$, (**Fc-FA-AQ**+C_{60})$_n$, and (C_{60})$_n$ films, we used OTE/SnO_2/(**FA-AQ**+C_{60})$_n$, OTE/SnO_2/(**Fc-FA-AQ**+C_{60})$_n$, and OTE/SnO_2/(C_{60})$_n$ as a photoanode in a photoelectrochemical cell. Photocurrent measurements were performed in acetonitrile containing NaI (0.5 M) and I_2 (0.01 M) as redox electrolyte and a Pt gauge counter electrode.

The IPCE values were calculated by normalizing the photocurrent values for incident light energy and intensity and using eq 3:[41b]

$$\text{IPCE}\ (\%) = 100 \times 1240 \times i_{sc}/(I_{inc} \times \lambda) \qquad (3)$$

where i_{sc} is the short circuit photocurrent (A/cm^2), I_{inc} is the incident light intensity (W/cm^2), and λ is the wavelength (nm).

The overall response of OTE/SnO_2/(**FA-AQ**+C_{60})$_n$ [spectrum (ii) in Figure 10a] parallels the broad absorption spectral

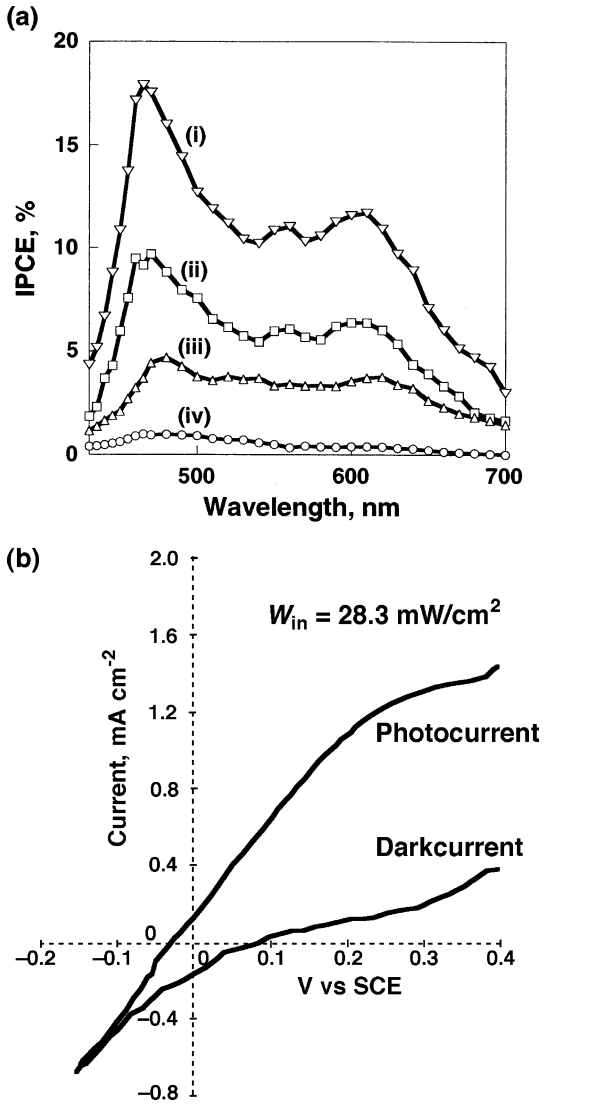

Figure 10. (a) The photocurrent action spectrum (presented in terms of % IPCE) of OTE/SnO_2/(**FA-AQ**+C_{60})$_n$ (i) at an applied bias potential of 0.2 V vs SCE and (ii) with no applied bias potential (iii) OTE/SnO_2/(C_{60})$_n$ with no applied bias potential and (iv) OTE/SnO_2/(**Fc-FA-AQ**+C_{60})$_n$ with no applied bias potential; electrolyte: 0.5 M NaI and 0.01M I_2 in acetonitrile. (b) $I-V$ characteristics of OTE/SnO_2/(**FA-AQ**+C_{60})$_n$ prepared from cluster solution of ([**FA-AQ**] = [C_{60}] = 0.31 mM) under visible light (λ > 370 nm) illumination; electrolyte: 0.5 M NaI and 0.01 M I_2 in acetonitrile, input power: 28.3 mW/cm^2.

features, indicating the involvement of both **FA-AQ** and C_{60} in the photocurrent generation to afford the maximum IPCE value as 9.7% at 470 nm. This value is significantly larger than the maximum IPCE value for OTE/SnO_2/(C_{60})$_n$ (4.7%) at 480 nm (spectrum (iii) in Figure 10a). In contrast, the maximum IPCE value of OTE/SnO_2/(**Fc-FA-AQ**+C_{60})$_n$ (0.98%) at 465 nm (spectrum (iv) in Figure 10a) is significantly smaller than that for OTE/SnO_2/ (C_{60})$_n$.

The CS step in the OTE/SnO_2/(**FA-AQ**+C_{60})$_n$ electrode can be further modulated by the application of an electrochemical bias.[41b] Figure 10b shows $I-V$ characteristics of the OTE/SnO_2/(**FA-AQ**+C_{60})$_n$ electrode under the visible light illumination. The photocurrent increases as the applied potential is scanned toward more positive potentials. Increased charge separation and the facile transport of charge carriers under positive bias are responsible for enhanced photocurrent generation. The IPCE value of OTE/SnO_2/(**FA-AQ**+C_{60})$_n$ at an applied bias potential

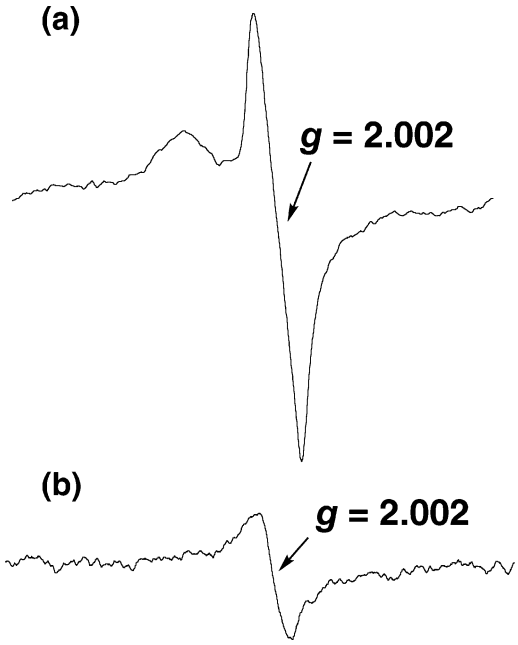

Figure 11. ESR spectra of (a) photoirradiated (**FA-AQ**+C_{60})$_n$ ([**FA-AQ**] = 0.31 mM; [C_{60}] = 0.31 mM) with a high-pressure mercury lamp and (b) photoirradiated (**Fc-FA-AQ**+C_{60})$_n$ ([**Fc-FA-AQ**] = 0.31 mM; [C_{60}] = 0.31 mM) in acetonitrile/toluene (3:1, v/v) with a high-pressure mercury lamp, measured at 123 K.

of 0.2 V vs SCE increases up to 17.9% at 465 nm [(i) in Figure 10a] corresponding to $I-V$ characteristics in Figure 10b.[45]

In the case of the OTE/SnO_2/(C_{60})$_n$ system, photoinduced electron transfer between the iodide ion and the excited state of C_{60} clusters is the primary step in the photocurrent generation, followed by injection of electrons from the radical anion of C_{60} clusters into SnO_2 nanocrystallites.[40a,41b] In the OTE/SnO_2/(**FA-AQ**+C_{60})$_n$ system, photoinduced electron transfer from FA to AQ and C_{60} in addition to photoinduced electron transfer from the iodide ion to C_{60} contributes an increase in the photocurrent generation as compared with the OTE/SnO_2/(C_{60})$_n$ system. In the case of the OTE/SnO_2/(**Fc-FA-AQ**+C_{60})$_n$ system, however, the fast back electron transfer from $AQ^{\bullet-}$ to Fc^+ in **Fc**$^+$**-FA-AQ**$^{\bullet-}$ as compared with that in **FA**$^{\bullet+}$**-AQ**$^{\bullet-}$ (vide supra) and also from the radical anion of $C_{60}^{\bullet-}$ to Fc^+ results in a decrease in the photocurrent generation as compared with the OTE/SnO_2/(C_{60})$_n$ system.

The existence of the radical ion pair (**FA**$^{\bullet+}$**-AQ** and $C_{60}^{\bullet-}$) in (**FA-AQ**+C_{60})$_n$ clusters upon photoexcitation is confirmed by ESR measurements in frozen acetonitrile/toluene (3:1, v/v). The ESR spectrum of photoirradiated (**FA-AQ**+C_{60})$_n$ composite clusters in frozen acetonitrile/toluene at 123 K is shown in Figure 11a. The ESR spectrum consists of two signals, one of which is attributable to $C_{60}^{\bullet-}$ at a small g value (g = 2.002) by the comparison of the ESR signal with that of the radical anion of C_{60} clusters, produced independently via the photoinduced electron transfer from dimeric 1-benzyl-1,4-dihydronicotinamide to C_{60} clusters.[16b,46,47] The other signal at a higher g value is thereby ascribed to **FA**$^{\bullet+}$**-AQ**. A similar ESR signal is observed for the photoirradiated (**Fc-FA-AQ**+C_{60})$_n$ composite clusters in frozen acetonitrile/toluene at 123 K (Figure 11b). In this case, however, the ESR signal intensity is significantly smaller than that observed for (**FA-AQ**+C_{60})$_n$ composite clusters (Figure 11a), because of the fast back electron transfer from the radical anion of C_{60} clusters to **Fc**$^+$**-FA-AQ**.[48]

In conclusion, an extremely long-lived CS state attained in **FA**$^{\bullet+}$**-AQ**$^{\bullet-}$ is drastically shortened in **Fc**$^+$**-FA-AQ**$^{\bullet-}$ by attaching the ferrocene unit, which has a larger reorganization energy of electron transfer than that of the FA moiety, due to a significant decrease in the CR driving force despite the longer CS distance. Such a drastic difference in their CS lifetimes also results in an opposite effect on the photoelectochemical properties of the composite films of **FA-AQ** and **Fc-FA-AQ** with fullerene clusters: **FA-AQ** enhances the photocurrent generation in OTE/SnO_2/(**FA-AQ**+C_{60})$_n$ as compared with OTE/SnO_2/(C_{60})$_n$, whereas **Fc-FA-AQ** retards the photocurrent generation.

Acknowledgment. This work was partially supported by a Grant-in-Aid (No. 16205020) from the Ministry of Education, Culture Sports, Science and Technology, Japan, and by the Academy of Finland and the National Technology Agency of Finland. P.V.K. acknowledges the support from the Office of Basic Energy Science of the U.S. Department of Energy. This is contribution No. NDRL 4466 from the Notre Dame Radiation Laboratory and from Osaka University.

Supporting Information Available: Photocurrent and photovoltage response action spectra and the power characteristics of OTE/SnO_2/(**FA-AQ**+C_{60})$_n$ electrode (S1). This material is available free of charge via the Internet at http://pubs.acs.org.

References and Notes

(1) (a) *The Photosynthetic Reaction Center*; Deisenhofer, J., Norris, J. R., Eds.; Academic Press: San Diego, 1993. (b) *Anoxygenic Photosynthetic Bacteria*; Blankenship, R. E., Madigan, M. T., Bauer, C. E., Eds.; Kluwer Academic Publishing: Dordrecht, 1995.

(2) (a) Wasielewski, M. R. In *Photoinduced Electron Transfer*; Fox, M. A., Chanon, M., Eds.; Elsevier: Amsterdam, 1988; Part A, pp 161−206. (b) Wasielewski, M. R. *Chem. Rev.* **1992**, *92*, 435. (c) Wasielewski, M. R.; Wiederrecht, G. P.; Svec, W. A.; Niemczyk, M. P. *Sol. Energy Mater. Sol. Cells* **1995**, *38*, 127.

(3) (a) Paddon-Row, M. N. *Acc. Chem. Res.* **1994**, *27*, 18. (b) Jordan, K. D.; Paddon-Row, M. N. *Chem. Rev.* **1992**, *92*, 395.

(4) Verhoeven, J. W. *Adv. Chem. Phys.* **1999**, *106*, 603.

(5) (a) Osuka, A.; Mataga, N.; Okada, T. *Pure Appl. Chem.* **1997**, *69*, 797. (b) Maruyama, K.; Osuka, A.; Mataga, N. *Pure Appl. Chem.* **1994**, *66*, 867.

(6) (a) Gust, D.; Moore, T. A.; Moore, A. L. *Acc. Chem. Res.* **1993**, *26*, 198. (b) Gust, D.; Moore, T. A.; Moore, A. L.; Lee, S.-J.; Bittersmann, E.; Luttrull, D. K.; Rehms, A. A.; DeGraziano, J. M.; Ma, X. C.; Gao, F.; Belford, R. E.; Trier, T. T. *Science* **1990**, *248*, 199. (c) Moser, C. C.; Keske, J. M.; Warncke, K.; Farid, R. S.; Dutton, P. L. *Nature* **1992**, *355*, 796. (d) Page, C. C.; Moser, C. C.; Chen, X.; Dutton, P. L. *Nature* **1999**, *402*, 47.

(7) (a) Chambron, J.-C.; Chardon-Noblat, S.; Harriman, A.; Heitz, V.; Sauvage, J.-P. *Pure Appl. Chem.* **1993**, *65*, 2343. (b) Blanco, M.-J.; Consuelo Jiménez, M.; Chambron, J.-C.; Heitz, V.; Linke, M.; Sauvage, J.-P. *Chem. Soc. Rev.* **1999**, *28*, 293. (c) Chambron, J.-C.; Collin, J.-P.; Dalbavie, J.-O.; Dietrich-Buchecker, C. O.; Heitz, V.; Odobel, F.; Solladie, N.; Sauvage, J.-P. *Coord. Chem. Rev.* **1998**, *178*−*180*, 1299. (d) Harriman, A.; Sauvage, J.-P. *Chem. Soc. Rev.* **1996**, *25*, 41.

(8) (a) Lewis, F. D.; Liu, X.; Liu, J.; Miller, S. E.; Hayes, R. T.; Wasielewski, M. R. *Nature* **2000**, *406*, 51. (b) Lewis, F. D.; Letsinger, R. L.; Wasielewski, M. R. *Acc. Chem. Res.* **2001**, *34*, 159.

(9) (a) Balzani, V.; Juris, A.; Venturi, M.; Campagna, S.; Serroni, S. *Chem. Rev.* **1996**, *96*, 759. (b) Arkin, M. R.; Stemp, E. D. A.; Holmlin, R. E.; Barton, J. K.; Hormann, A.; Olson, E. J. C.; Barbara, P. F. *Science* **1996**, *273*, 475.

(10) (a) Fukuzumi, S.; Guldi, D. M. In *Electron Transfer in Chemistry*; Balzani, V. Ed.; Wiley-VCH: Weinheim, 2001; Vol. 2, pp 270−337. (b) Fukuzumi, S. *Org. Biomol. Chem.* **2003**, *1*, 609.

(11) (a) Imahori, H.; Guldi, D. M.; Tamaki, K.; Yoshida, Y.; Luo, C.; Sakata Y.; Fukuzumi, S. *J. Am. Chem. Soc.* **2001**, *123*, 6617. (b) Guldi, D. M.; Imahori, H.; Tamaki, K.; Kashiwagi, Y.; Yamada, H.; Sakata, Y.; Fukuzumi, S. *J. Phys. Chem. A* **2004**, *108*, 541. (c) Imahori, H.; Sekiguchi, Y.; Kashiwagi, Y.; Sato, T.; Araki, Y.; Ito, O.; Yamada, H.; Fukuzumi, S. *Chem. Eur. J.* **2004**, *10*, 3184.

(12) (a) Marcus, R. A. *Annu. Rev. Phys. Chem.* **1964**, *15*, 155. (b) Marcus, R. A. *Angew. Chem., Int. Ed. Engl.* **1993**, *32*, 1111. (c) Marcus, R. A.; Sutin, N. *Biochim. Biophys. Acta* **1985**, *811*, 265.

(13) (a) Fukuzumi, S.; Ohkubo, K.; Imahori, H.; Shao, J.; Ou, Z.; Zheng, G.; Chen, Y.; Pandey, R. K.; Fujitsuka, M.; Ito, O.; Kadish, K. M. *J. Am. Chem. Soc.* **2001**, *123*, 10676. (b) Ohkubo, K.; Kotani, H.; Shao, J.; Ou,

Z.; Kadish, K. M.; Li, G.; Pandey, R. K.; Fujitsuka, M.; Ito, O.; Imahori, H.; Fukuzumi, S. *Angew. Chem., Int. Ed.* **2004**, *43*, 853.

(14) Fukuzumi, S. Kotani, H.; Ohkubo, K.; Ogo, S.; Tkachenko, N. V.; Lemmetyinen, H. *J. Am. Chem. Soc.* **2004**, *126*, 1600.

(15) Bedja, I.; Hotchandani, S.; Kamat, P. V. *J. Phys. Chem.* **1994**, *98*, 4133.

(16) (a) Wallenfels, K.; Gellrich, M. *Chem. Ber.* **1959**, *92*, 1406. (b) Fukuzumi, S.; Suenobu, T.; Patz, M.; Hirasaka, T.; Itoh, S.; Fujitsuka, M.; Ito, O. *J. Am. Chem. Soc.* **1998**, *120*, 8060.

(17) Photochemical properties of **Fc-FA-AQ** in PhCN were reported previously; Okamoto, K.; Araki, Y.; Ito, O.; Fukuzumi, S. *J. Am. Chem. Soc.* **2004**, *126*, 56.

(18) Tkachenko, N. V.; Rantala, L.; Tauber, A. Y.; Helaja, J.; Hynninen, P. H.; Lemmetyinen, H. *J. Am. Chem. Soc.* **1999**, *121*, 9378.

(19) Luo, C.; Fujitsuka, M.; Watanabe, A.; Ito, O.; Gan, L.; Huang, Y.; Huang, C.-H. *J. Chem. Soc., Faraday Trans.* **1998**, *94*, 527.

(20) The SHACV method provides a superior approach to directly evaluating the one-electron redox potentials in the presence of a follow-up chemical and reaction, relative to the better-known dc and fundamental harmonic ac methods. See: (a) McCord, T. G.; Smith, D. E. *Anal. Chem.* **1969**, *41*, 1423. (b) Bond, A. M.; Smith, D. E. *Anal. Chem.* **1974**, *46*, 1946. (c) Wasielewski, M. R.; Breslow, R. *J. Am. Chem. Soc.* **1976**, *98*, 4222. (d) Arnett, E. M.; Amarnath, K.; Harvey, N. G.; Cheng, J. *J. Am. Chem. Soc.* **1990**, *112*, 344. (e) Okamoto, K.; Imahori, H.; Fukuzumi, S. *J. Am. Chem. Soc.* **2003**, *125*, 7014.

(21) Mann, C. K.; Barnes, K. K. *Electrochemical Reactions in Nonaqueous Systems*; Marcel Dekker: New York, 1990.

(22) (a) Becke, A. D. *J. Chem. Phys.* **1993**, *98*, 5648. (b) Lee, C.; Yang, W.; Parr, R. G. *Phys. Rev. B* **1988**, *37*, 785. (c) Hehre, W. J.; Radom, L.; Schleyer, P. v. R.; Pople, J. A. *Ab Initio Molecular Orbital Theory*; Wiley: New York, 1986.

(23) Frisch, M. J.; Trucks, G. W.; Schlegel, H. B.; Scuseria, G. E.; Robb, M. A.; Cheeseman, J. R.; Zakrzewski, V. G.; Montgomery, J. A., Jr.; Stratmann, R. E.; Burant, J. C.; Dapprich, S.; Millam, J. M.; Daniels, A. D.; Kudin, K. N.; Strain, M. C.; Farkas, O.; Tomasi, J.; Barone, V.; Cossi, M.; Cammi, R.; Mennucci, B.; Pomelli, C.; Adamo, C.; Clifford, S.; Ochterski, J.; Petersson, G. A.; Ayala, P. Y.; Cui, Q.; Morokuma, K.; Malick, D. K.; Rabuck, A. D.; Raghavachari, K.; Foresman, J. B.; Cioslowski, J.; Ortiz, J. V.; Baboul, A. G.; Stefanov, B. B.; Liu, G.; Liashenko, A.; Piskorz, P.; Komaromi, I.; Gomperts, R.; Martin, R. L.; Fox, D. J.; Keith, T.; Al-Laham, M. A.; Peng, C. Y.; Nanayakkara, A.; Gonzalez, C.; Challacombe, M.; Gill, P. M. W.; Johnson, B.; Chen, W.; Wong, M. W.; Andres, J. L.; Gonzalez, C.; Head-Gordon, M.; Replogle, E. S.; Pople, J. A. *Gaussian 98 (Revision A.7)*; Gaussian, Inc.: Pittsburgh, PA, 1998.

(24) The singlet and triplet excited energy of AQ has been reported as 2.85 eV (^{1}AQ*) and 2.45 eV (^{3}AQ*). See: Itoh, T.; Yamaji, M.; Shizuka, H. *Spectrochim. Acta, Part A* **2002**, *58*, 397.

(25) The time component spectrum with a lifetime of 0.4 ps indicating the absorption rise is affected by the overlap with the decay of the singlet absorption in the long wavelength region (λ_{max} = 720 nm).

(26) Hubig, S. M.; Bockman, T. M.; Kochi, J. K. *J. Am. Chem. Soc.* **1997**, *119*, 2926.

(27) Hamanoue, K.; Nakayama, T.; Tsujimoto, I.; Miki, S. Ushida, K. *J. Phys. Chem.* **1995**, *99*, 5802.

(28) Patel, K. B.; Willson, R. L. *J. Chem. Soc., Faraday Trans. 1* **1973**, *69*, 814.

(29) Roberts, J. L., Jr.; Sugimoto, H.; Barrette, W. C., Jr.; Sawyer, D. T. *J. Am. Chem. Soc.* **1985**, *107*, 4556.

(30) Yoshihara, T.; Yamaji, M.; Itoh, T.; Shizuka, H.; Shimokage, T.; Tero-Kubota, S. *Phys. Chem. Chem. Phys.* **2000**, *2*, 993.

(31) For the absorption maxima of radical anions of anthraquinone derivatives, see: Fujita, M.; Ishida, A.; Majima, T.; Takamuku, S. *J. Phys. Chem.* **1996**, *100*, 5382.

(32) The absorption band due to the $FA^{\bullet+}$ moiety is overlapped with that due to the $AQ^{\bullet-}$ moiety, since the absorption band due to the aniline radical cation is known to have the absorption between 500 and 700 nm; see: Sakata, T.; Okai, T.; Sugimoto, H.; Tsubomura, H. *Bull. Chem. Soc. Jpn.* **1975**, *48*, 2945.

(33) Bernasconi, C. F.; Ketner, R. J. *J. Org. Chem.* **1998**, *63*, 6266.

(34) For the transient absorption spectrum of $Me_2An^{\bullet+}$, see: (a) Lee, K.; Falvey, D. E. *J. Am. Chem. Soc.* **2000**, *122*, 9361. (b) Fukuzumi, S.; Nakanishi, I.; Tanaka, K. *J. Phys. Chem. A* **1999**, *103*, 11212.

(35) The excited state of Fc cannot be formed since the extinction coefficient for Fc at 355 nm is very small; see: Ding, W.; Sanderson, C. T.; Conover, R. C.; Johnson, M. K.; Amster, I. J.; Kutal, C. *Inorg. Chem.* **2003**, *42*, 1532. The triplet excited energy of ferrocene (1.68 eV) is much higher than CS energy in **Fc-FA-AQ** (1.16 eV); see: Darmanyan, A. P.; Jenks, W. S.; Eloy, D.; Jardon, P. *J. Phys. Chem. B* **1999**, *103*, 3323.

(36) The transient component spectrum of **Fc-FA-AQ** with the lifetime of 0.7 ps in Figure 6a, which corresponds to the triplet excited state (**Fc-FA-^{3}AQ***), has a similar absorption maximum around 600 nm, but not exactly the same as that of **FA-^{3}AQ*** with the lifetime of 1.7 ps in Figure 2, probably due to the different contribution of the fast rise and decay of the absorption due to the singlet excited state (^{1}AQ*) between **Fc-FA-AQ** and **FA-AQ**.

(37) (a) Fukuzumi, S.; Yoshida, Y.; Okamoto, K.; Imahori, H.; Araki, Y.; Ito, O. *J. Am. Chem. Soc.* **2002**, *124*, 6794. (b) Fukuzumi, S.; Okamoto, K.; Yoshida, Y.; Imahori, H.; Araki, Y.; Ito, O. *J. Am. Chem. Soc.* **2003**, *125*, 1007. (c) Fukuzumi, S.; Okamoto, K.; Imahori, H. *Angew. Chem., Int. Ed.* **2002**, *41*, 620.

(38) Yang, E. S.; Chan, M.-S.; Wahl, A. C. *J. Phys. Chem.* **1980**, *84*, 3094.

(39) Eberson, L. *Electron-Transfer Reactions in Organic Chemistry*; Springer-Verlag: Heidelberg, 1987.

(40) (a) Kamat, P. V.; Barazzouk, S.; Thomas, K. G.; Hotchandani, S. *J. Phys. Chem. B* **2000**, *104*, 4014. (b) Sudeep P. K.; Ipe, B. I.; Thomas, K. G.; George, M. V.; Barazzouk, S.; Hotchandani, S.; Kamat, P. V. *Nano Lett.* **2002**, *2*, 29. (c) Kamat, P. V.; Barazzouk, S.; Hotchandani, S.; Thomas, K. G. *Chem. Eur. J.* **2000**, *6*, 3914. (d) Barazzouk, S.; Hotchandani, S.; Kamat, P. V. *Adv. Mater.* **2001**, *13*, 1614.

(41) (a) Hasobe, T.; Imahori, H.; Fukuzumi, S.; Kamat, P. V. *J. Phys. Chem. B* **2003**, *107*, 12105. (b) Hasobe, T.; Imahori, H.; Fukuzumi, S.; Kamat, P. V. *J. Mater. Chem.* **2003**, *13*, 2515.

(42) (a) Hasobe, T.; Imahori, H.; Kamat, P. V.; Fukuzumi, S. *J. Am. Chem. Soc.* **2003**, *125*, 14962. (b) Hasobe, T.; Kashiwagi, Y.; Absalom, M. A.; Sly, J.; Hosomizu, K.; Crossley, M. J.; Imahori, H.; Kamat, P. V.; Fukuzumi, S. *Adv. Mater.* **2004**, *16*, 975. (c) Hasobe, T.; Hattori, S.; Kotani, H.; Ohkubo, K.; Hosomizu, K.; Imahori, H.; Kamat, P. V.; Fukuzumi, S. *Org. Lett.* **2004**, *6*, 3103.

(43) (a) Fukuzumi, S.; Ohkubo, K.; Tokuda, Y.; Suenobu, T. *J. Am. Chem. Soc.* **2000**, *122*, 4286. (b) Mulliken, R. S.; Person, W. B. *Molecular Complexes*; A Lecture and Reprint Volume; Wiley-Interscience: New York, 1969. (c) Foster, R. *Organic Charge-Transfer Complexes*; Academic Press: New York, 1969.

(44) (a) D'Souza, F.; Gadde, S.; Zandler, M. E.; Arkady, K.; El-Khouly, M. E.; Fujitsuka, M.; Ito, O. *J. Phys. Chem. A* **2002**, *106*, 12393. (b) Schuster, D. I.; Jarowski, P. D.; Kirschner, A. N.; Wilson, S. R. *J. Mater. Chem.* **2002**, *12*, 2041. (c) Tkachenko, N. V.; Rantala, L.; Tauber, A. Y.; Helaja, J.; Hynninen, P. H.; Lemmetyinen, H. *J. Am. Chem. Soc.* **1999**, *121*, 9378.

(45) Photocurrent response, photovoltage response of OTE/SnO_2/(**FA-AQ**+C_{60})$_n$, and power characteristics of the photoelectrochemical cell are shown in Supporting Information S1.

(46) The slightly larger *g* value (2.002) in $FA^{\bullet+}$-$AQ^{\bullet-}$ as compared to the *g* value of the radical anion of C_{60} cluster (2.001) may result from the $\pi-\pi$ interaction of $C_{60}^{\bullet-}$ with formanilide or ferrocene moiety as shown in Figure 7. Such an interaction lowers the symmetry of $C_{60}^{\bullet-}$, resulting in an increase in the *g* value; see: Fukuzumi, S.; Mori, H.; Suenobu, T.; Imahori, H.; Gao, X.; Kadish, K. M. *J. Phys. Chem. A* **2000**, *104*, 10688.

(47) Hasobe, T.; Imahori, H.; Kamat, P. V.; Ahn, T. K.; Kim, S. K.; Kim, D.; Fujimoto, A.; Hirakawa, T.; Fukuzumi, S. *J. Am. Chem. Soc.* **2005**, *127*, 1216.

(48) The significant difference in the ESR signal intensities between photoirradiated two samples: (**FA-AQ**+C_{60})$_n$ and (**Fc-FA-AQ**+C_{60})$_n$ in Figure 11 is quite consistent with that of IPCE values in the composite films between OTE/SnO_2/(**FA-AQ**+C_{60})$_n$ and OTE/SnO_2/(**Fc-FA-AQ**+C_{60})$_n$.